Title	The study of high-efficiency pion production
Author(s)	Yao, Weichao; Aoki, Masaharu; Wu, Chen et al.
Citation	European Physical Journal Plus. 2025, 140, p. 267
Version Type	VoR
URL	https://hdl.handle.net/11094/101111
rights	This article is licensed under a Creative Commons Attribution 4.0 International License.
Note	

Eur. Phys. J. Plus (2025) 140:267
https://doi.org/10.1140/epjp/s13360-025-06164-9

THE EUROPEAN
PHYSICAL JOURNAL PLUS

Regular Article

The study of high-efficiency pion production

Weichao Yao[1,a], **Masaharu Aoki**[1], **Chen Wu**[2,3], **Kou Oishi**[4,5], **Yoshinori Fukao**[4]

[1] Department of Physics, Graduate School of Science, Osaka University, Osaka 560043, Japan
[2] Institute of High Energy Physics, Chinese Academy of Sciences, Beijing 100049, China
[3] Spallation Neutron Source Science Center, Dongguan 523808, China
[4] High Energy Accelerator Research Organization (KEK), Tsukuba, Japan
[5] Imperial College London, London, UK

Received: 15 October 2024 / Accepted: 20 February 2025

Abstract An optimization study was conducted on low-energy pion production using a cylindrical tungsten target for the COMET Phase-II experiment, taking into account recent measurements of proton-beam emittance. The study suggests factor 1.6 of improvement in pion production efficiency by reducing the target radius down to 4 mm. This enhancement is attributed to the reduction in the emittance of the proton beam. Further increases in target radius simply reduce the yield of low-energy pions and, consequently, the stopping rate of low-energy muons in the muon stopping target. The analysis reveals that the pion production spectrum at higher momentum cannot compensate for the limitations imposed by the range–momentum curve of pions. There is a potential further improvement in low-energy pion production with an ideally narrow proton beam.

1 Introduction

The COMET (Coherent Muon to Electron Transition) experiment at the Japan Proton Accelerator Research Complex (J-PARC) aims to investigate the coherent $\mu^- + N \rightarrow e^- + N$ conversion in a nuclear field. This experiment represents a next-generation rare muon decay experiment in the discipline of high-intensity particle physics. The COMET experiment is divided into two stages: Phase-I and Phase-II [1, 2]. This paper focuses on Phase-II that follows Phase-I and aims to achieve an upper limit sensitivity of $\leq 7 \times 10^{-17}$ at 90% confidence level (C.L.), which is a significant advancement over SINDRUM-II measurements [3]. Achieving this sensitivity necessitates a high-intensity muon beam, which, in turn, demands an exceptionally intense pion source, as muons are produced by pion decay. Pions are produced by protons striking a production target, where its production threshold in the laboratory system is approximately 290 MeV. J-PARC is set to deliver a proton beam with a beam power of 56 kW at a kinetic energy of 8 GeV for Phase-II. To effectively suppress high-momentum background particles, a backward-scattered pion capture scheme has been implemented.

A critical aspect of optimizing the experimental setup involves an intensive study of the production target, aimed at enhancing pion production efficiency. This study endeavors to achieve this by comprehensively investigating pion–nucleon interactions and ionization energy loss in a target. Initially, Monte Carlo (MC) simulation was used to optimize the target radius, resulting in a significant improvement in pion production efficiency. Subsequently, we introduce a simple model to explain the behavior of low-energy pion yield.

The paper is organized as follows: Sect. 2 provides an overview of the Phase-II experiment. Section 3 describes the proton-beam emittance at J-PARC. Section 4 presents the MC simulation for the COMET experiment Phase-II. Section 5 offers an analysis and results that reasonably explain the observed behavior from the full Monte Carlo calculation. Finally, the paper concludes with discussions.

2 COMET Phase-II

The layout of Phase-II, shown in Fig. 1, consists of several key components. A primary proton beam is directed toward a production target located inside the pion capture solenoid. Pions produced and emerged from the production target are then collected by a strong magnetic field of 5 T.

Only those pions directed toward the muon transport solenoid are captured. Given that high-energy pions, which do not contribute to the muon stopping rate but increase background noise, are predominantly produced in the forward direction, this configuration

---

[a] e-mail: yaowc@ihep.ac.cn (corresponding author)

Fig. 1 Experimental layout of COMET Phase-II

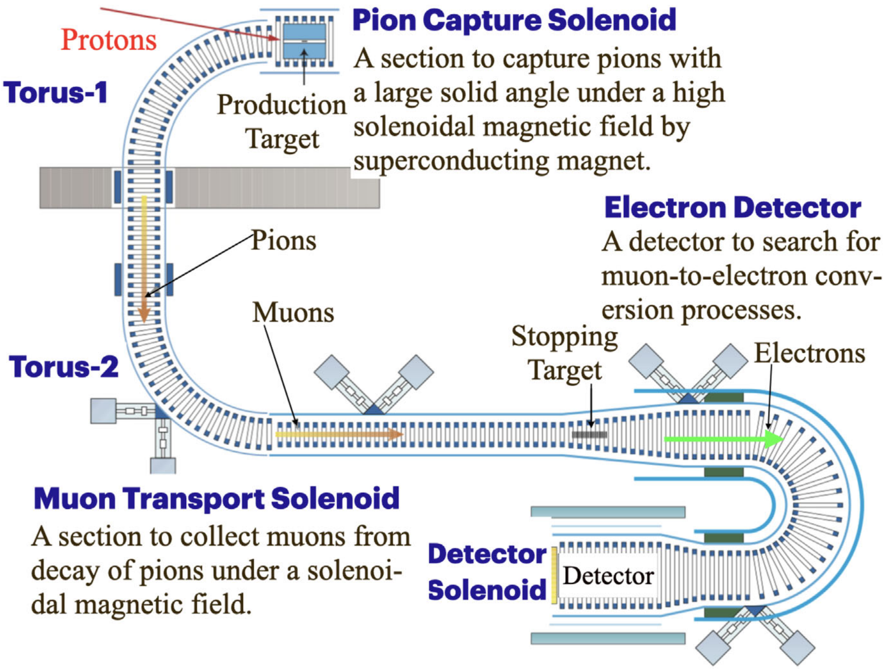

Fig. 2 (Left) the momentum spectrum of muons stopping in the muon stopping target. (Right) the momentum distribution of pions that produce the muons stopping in the muon stopping target at the position of the surface of the production target

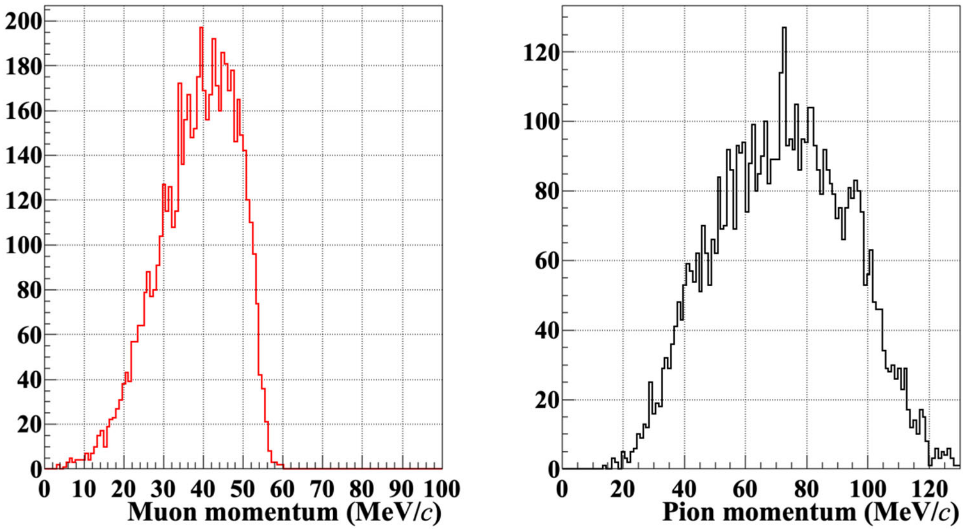

presents a distinct advantage in mitigating the influx of high-energy pions into the muon transport solenoid. Pions collected by the pion capture solenoid are guided to the muon transport solenoid, where they decay to muons.

A portion of these low-energy muons is subsequently stopped in an aluminum muon stopping target and utilized for the muon to electron conversion search. The electrons emitted from the muon stopping target are measured using an electron detector. Since the experimental sensitivity primarily depends on the muon stopping rate, optimizing the system to maximize the muon stopping rate is crucial.

Various factors influence the muon stopping rate, including the material and dimensions of the production target, the strength of the magnetic field, the design of the beam collimator in the muon transport solenoid, and the arrangement of the muon stopping target.

To achieve better signal electron energy resolution, the muon stopping target is divided into 25 thin disks, each disk restricted to a thickness of 0.2 mm, with a radius of 100 mm, resulting in a total thickness of 13.5 g/cm^2 along the beam axis. As shown in Fig. 2(left), only muons with momentum smaller than 60 MeV/c can be stopped in the muon stopping target. The momentum distribution of pions emerging from the production target and leading to muons that stop in the muon stopping target is shown in Fig. 2(right). These pions have momentum lower than 130 MeV/c (102 MeV/c for 90%).

The production target is cylindrical in shape. In a previous study, the target dimensions were optimized to have a radius of 10 mm and a length of 32 cm, resulting in a muon stopping rate of 1.6×10^{-3} per proton-on-target (POT), assuming a primary proton-beam

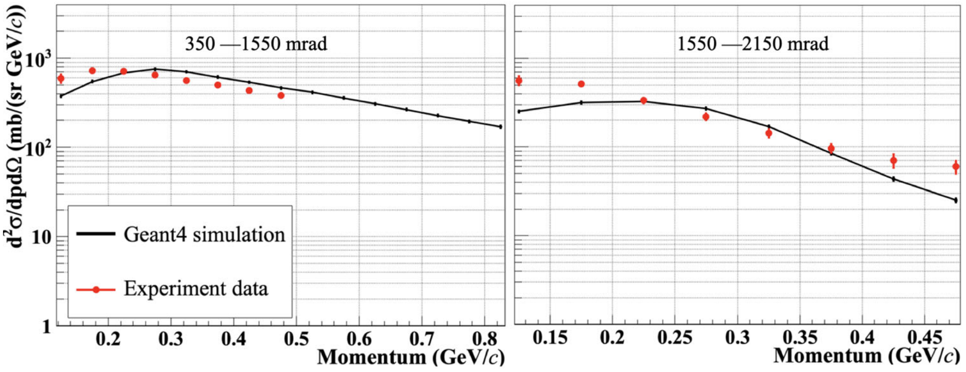

Fig. 3 Comparison of the measured double-differential π^- cross section for p-Cu interactions at 8 GeV/c with Geant4 results. The left figure shows forward production (350 mrad $\leq \theta <$ 1550 mrad), while the right figure shows backward production (1550 mrad $\leq \theta <$ 2150 mrad)

size of 5.8 mm and 2.9 mm in the horizontal and vertical direction, respectively [4]. Pions are to be emitted from the side due to the target's shape, making it crucial to optimize the target radius with respect to the proton-beam emittance.

3 Proton-beam emittance

The preliminary estimate in the Conceptual Design Report (CDR) [1] indicated that the emittance of the proton-beam extracted from the J-PARC Main Ring (MR) to the Hadron Hall was conservatively estimated to be within the range of 10–15 π mm · mrad at 8 GeV. The optimization of the target size in previous studies [4] was based on this estimation. However, a commissioning measurement of the 8-GeV proton beam at J-PARC in February 2018 revealed different values. During this commissioning, the measurement of protons extracted from the MR showed a 2σ emittance of 0.78 π mm · mrad and 4.6 π mm · mrad in the horizontal and vertical direction, respectively. The number of protons per bunch was the same as in Phase-I, with 3.2 kW, but the proton spill cycle was different (5.52 sec in the measurement, compared to 2.48 sec in Phase-I). Subsequently, the beam optics of the new proton beamline was calculated by the J-PARC group, resulting in beam spot sizes at the pion production target that are 1.4 mm horizontally and 1.0 mm vertically at 1σ [5]. For Phase-II, the beam power will be increased to 56 kW. We estimate an achievable proton beam with a 2σ emittance of 0.78 π mm · mrad (measurement) and 10.56 π mm · mrad (simulation [6]) in the horizontal and vertical directions. Based on reasonable beam optics between the MR extraction and the COMET target, the proton-beam spot size at the target is obtained from above emittance to be 1.46 mm and 1.36 mm in the horizontal and vertical direction, respectively, at 1σ.

This updated beam emittance is significantly smaller than the one originally assumed when COMET was designed. Given this deviation, it is essential to optimize the target shape and alignment accordingly.

4 Monte Carlo simulation

The re-optimization of the target radius was performed using Geant4-10.01 with the `QGSP_BERT_HP` hadron physics model. The simulation model consists of the production target, a series of solenoids connecting the pion capture solenoid to the detector solenoid, and the muon stopping target. To evaluate the applicability of the model at intermediate energies, the study considered the double-differential cross section for the production of negative pions in the kinematic range 0.1 GeV/c $\leq p_\pi \leq$ 0.8 GeV/c and 0.1 rad$\leq \theta_\pi \leq$2.15 rad from the collisions of protons of 8 GeV/c on copper target with a thickness of 0.18 g/cm^2. The pion yield was averaged over different momentum and angular ranges. A comparison between the measured double-differential π^- cross sections for proton–copper interactions at 8 GeV/c [7] and the results from GEANT4 using `QGSP_BERT_HP` hadron physics model is shown in Fig. 3. The π^- momentum and angular distributions at production for 8-GeV/c incident proton momenta are illustrated in Fig. 4.Figure 5 shows the muon stopping rate as a function of the radius of the pion production target. Notably, the maximum muon stopping rate is achieved with a 4 mm target radius, which is significantly smaller than the previously studied value of 10 mm.

The features observed in Fig. 5 reveal important insights into the optimization process. Below 4 mm, the rising curve is primarily due to the size of the proton-beam spot, which is directly influenced by the primary proton-beam emittance. Figure 6 shows the percentage of primary protons hitting the production target. The target radius should be larger than 4 mm so that most of the protons hit the target. Conversely, above 4 mm, the gradually decreasing slope reflects a compromise between factors such as pion absorption due to nuclear interaction, which decreases the total number of pions, and the energy loss of pions as they traverse the material, resulting in low-energy pions that serve as a source of stopping muons.

The discussion of these factors highlights the complex interplay among various parameters affecting the muon stopping rate. While larger target radii may initially seem beneficial, the nuanced effects of proton-beam characteristics and pion interactions must be carefully considered in the optimization process.

Fig. 4 The momentum and angular distribution of π^- production for 8-GeV/c incident proton momenta

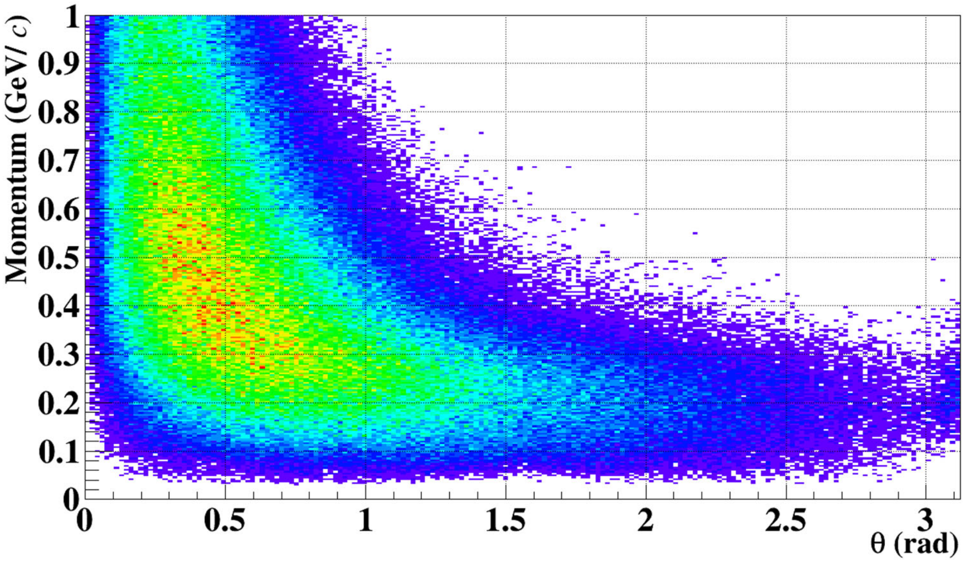

Fig. 5 The yield of the stopping muons as a function of the target radius

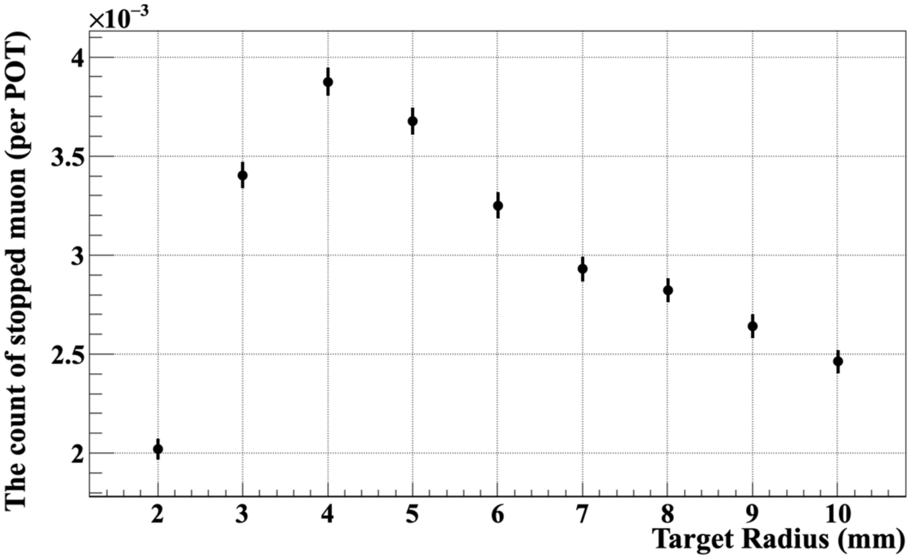

Fig. 6 The efficiency of the proton-beam striking the target

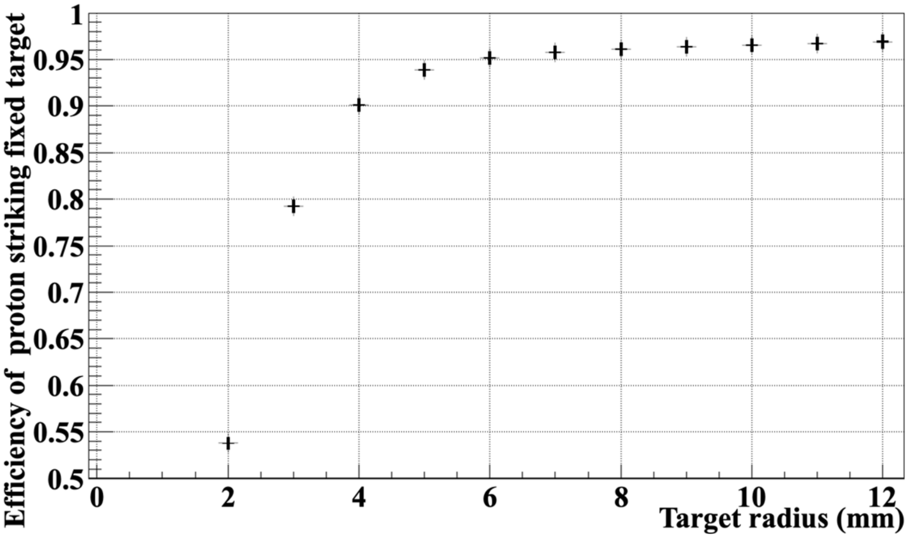

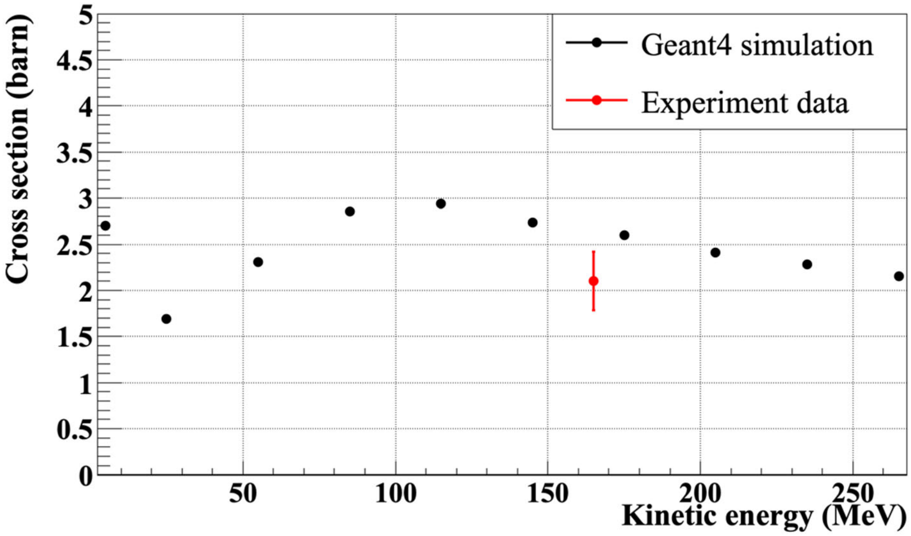

Fig. 7 The pion absorption cross section within tungsten as a function of the kinetic energy. The red point is a experiment data [12]

5 Pion interaction in material

Understanding the interaction of pions within the production target material is crucial for optimizing pion production efficiency. There are two major interaction processes. One is absorption due to nuclear interaction, where it is dominated by Δ resonance in this low-energy region [8–10]. The other is ionization energy loss [11].

5.1 Pion absorption through nucleus interaction

The typical nuclear absorption cross section is less than a few barns at the energy of Δ resonance, around 200 MeV in kinetic energy [10]. This amount of cross section results in only a few percent loss of pions for a 6 mm, and it cannot explain the decrease in the muon stopping rate observed between 4 mm and 10 mm, as shown in Fig. 5. To ensure that Geant4 with the `QGSP_BERT_HP` model does not overestimate the nuclear absorption phenomena, the cross-section data in Geant4 were extracted by impinging pions on a simple thin tungsten slab with a thickness of 0.1 mm. The electromagnetic interaction was turned off for this calculation. Figure 7 shows the result of the evaluation.

The experimental data of negative pion absorption from Ref. [12] are also shown in the same figure. Since they are reasonably consistent, we conclude that the gradual decreasing feature observed above a 4-mm production target radius in Fig. 5 is not dominated by nuclear absorption.

5.2 Ionization energy loss in tungsten

Figure 8 shows the spectrum of the initial pion momentum produced by an 8-GeV proton, calculated by Geant4 with `QGSP_BERT_HP`. To investigate whether the low-momentum pions increase by placing a momentum degrader, a simple Geant4 calculation impinging pions with this momentum spectrum into a slab was performed. The nuclear interaction was turned off for this calculation. Figure 9 shows the momentum spectra of pions passing through the degrader for three different thicknesses of the slab. The number of pions in the momentum region below 130 MeV/c simply decreases as the thickness of the degrader increases. Low-momentum pions are stopped in the degrader due to ionization energy loss, while high-momentum pions are degraded into low-momentum pions through the same process. However, there are not enough pions feeding in from the higher momentum region to compensate for these losses.

5.3 Range–momentum curve of pions in tungsten

To understand why placing a degrader increases neither low-momentum pions nor the muon stopping rate, the study examined the total distance pions travel through a material before coming to rest. A range–momentum curve [13] of low-momentum pions was calculated using Geant4 with only electromagnetic interaction turned on. Figure 10 shows the result, calculated with the initial pion momentum shown in Fig. 8.A band of 4-mm range in Fig. 10 shall correspond to the pions of interest (less than 102 MeV/c) that produce muons stopped in the muon stopping target. For examples, pions within the range of (0, 4) mm are important when no degrader is inserted, and pions within the range of (10, 14) mm are important when a 10-mm degrader is inserted. Figure 11 shows a projection of Fig. 10 onto the range axis, indicating that the curve is a decreasing function. It is obvious that the insertion of any thickness of the degrader does not increase the stopped muon yield at all.

Fig. 8 The momentum spectrum of initial pions produced by 8-GeV protons striking a target (black solid histogram); a small peak at the momentum of around 180 MeV/c is due to $\Sigma^- \rightarrow n\pi^-$. The red dashed curve represents the differentiation of the path length of a charged particle for a given momentum, see the text in the discussion section

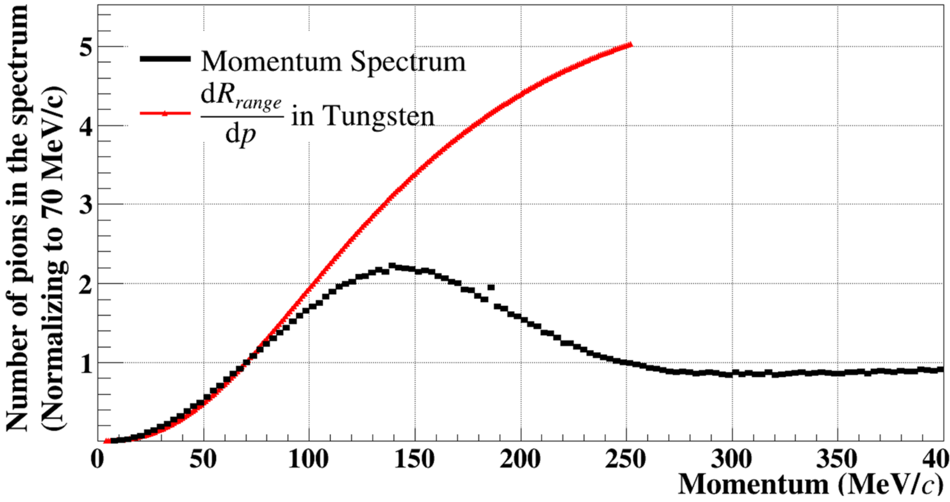

Fig. 9 The change of momentum spectrum of pions after passing through tungsten of different thickness. The solid black curve represents a thickness of 2 mm, the dotted red curve represents a thickness of 4 mm, and the dashed blue curve represents a thickness of 10 mm

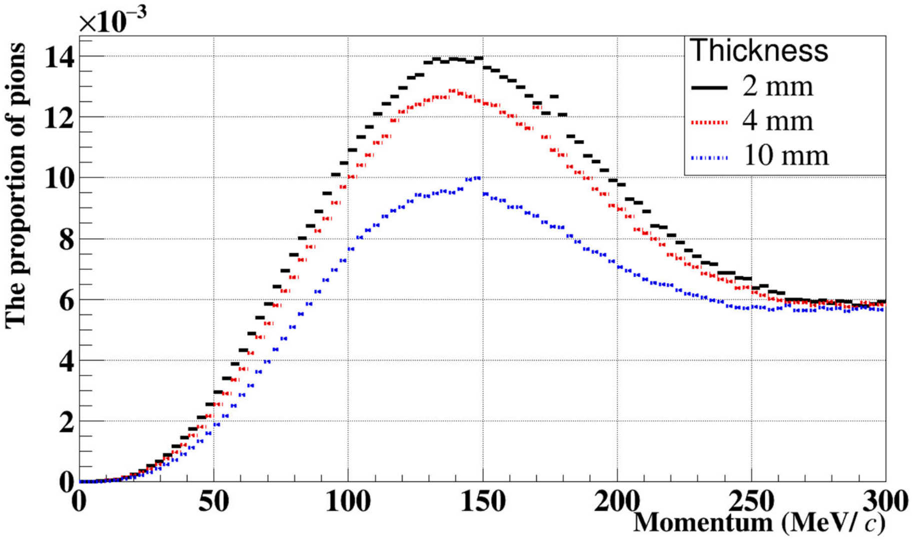

Fig. 10 The range–momentum curve of charged pions in tungsten. The initial momentum is as shown in Fig. 8

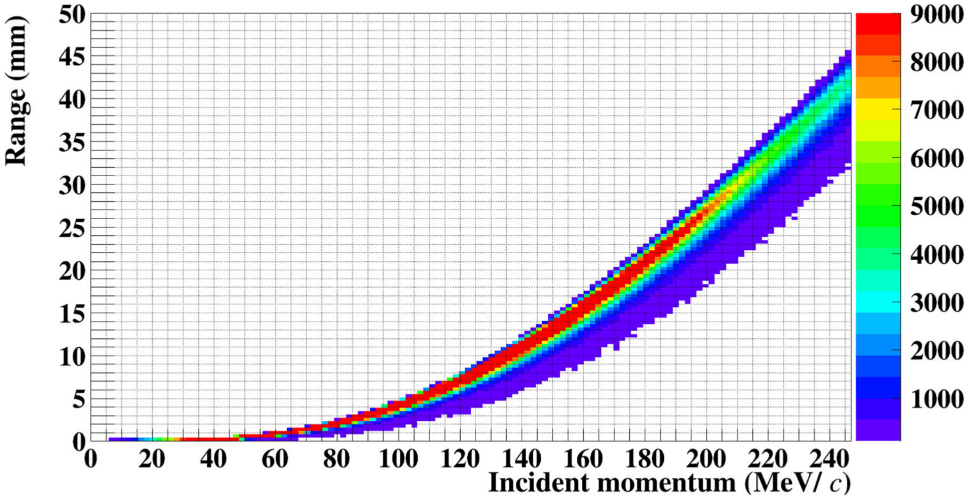

Let $n_\pi(R)$ be the density function of the plot shown in Fig. 11, the expected stopped muon yield can be approximately calculated by:

$$N_\mu(r_{\max}; d) = \int_0^{r_{\max}} N_\pi(r; r_{\max}, d) \cdot \exp^{-\Sigma(r_{\max}-r)} \cdot f_\pi(r) \mathrm{d}r, \tag{1}$$

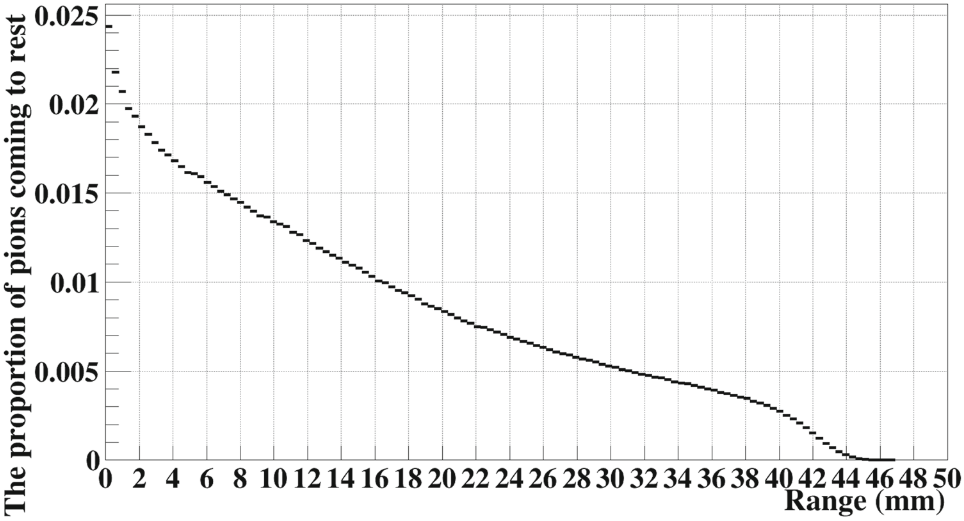

Fig. 11 Range distribution of pion, assuming the initial momentum in Fig. 8. Range is represented as a geometrical length for stopped pions in tungsten

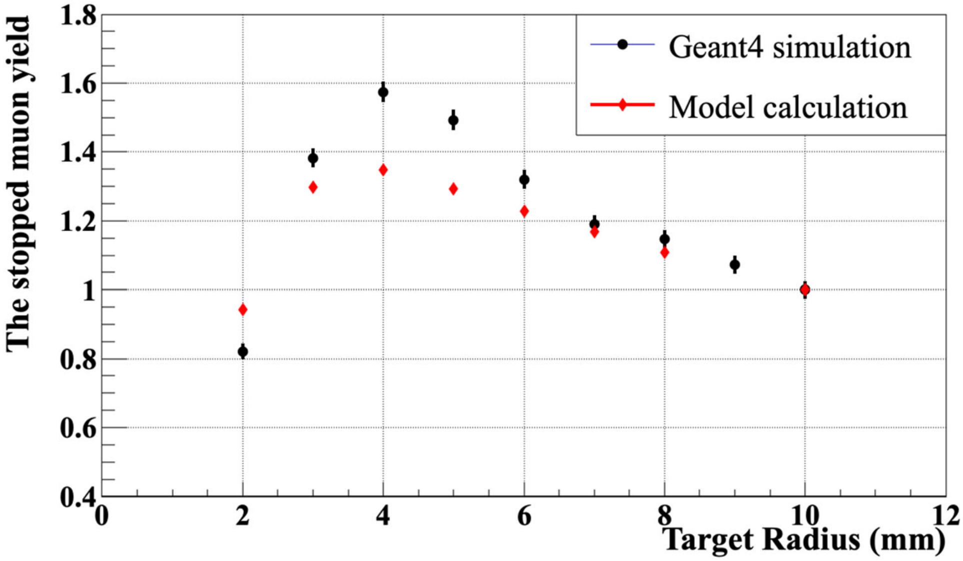

Fig. 12 The stopped muon yield as a function of target radius, with results normalized to a thickness of 10 mm. The black points represent the simulation results, while the red points represent the model calculations

$$N_\pi(r; r_{\max}, d) = \int_{r_{\max}-r}^{r_{\max}-r+d} n_\pi(R)\mathrm{d}R, \tag{2}$$

where $r_{\max}$ is the radius of the production target, d represents the band of the range that includes more than 90% of the pions of interest, $N_\pi(r; r_{\max},\ d)$ is the total number of pions of interest at $r_{max} - r$, Σ is the macroscopic nuclear interaction cross section (m^{-1}) for pions, and $f_\pi(r)$ is the pion production rate per POT at radial position r. Figure 12 shows the result of $N_\mu(r_{\max}; d = 4\ \text{ mm })$ calculation together with the overall Geant4 result. Both plots are normalized to have the same value at $r_{\max} = 10\ \text{ mm }$. The results remain fairly consistent, indicating that the model described above is valid.

6 Discussion

To investigate the conditions that could increase the stopped muon yield by inserting a degrader, we examine the range–momentum curve (Fig. 10). Assuming that the density function of the initial pion momentum spectrum is represented by $g(p)$ where p is the initial pion momentum, and the range of the pion for a given momentum is denoted by $R(p)$; the number of pions within a fixed width of the range ΔR is given by:

$$n_\pi(R)\Delta R = g(p)\Delta p, \tag{3}$$

where Δp is the corresponding width in the momentum domain. Thus,

$$n_\pi(R) = g(p)\frac{\mathrm{d}p}{\mathrm{d}R}. \tag{4}$$

If $n_\pi(R + R_d)$ is larger than $n_\pi(R)$, the muon stopping rate at $R + R_d$ is larger than at R. Therefore, inserting a degrader of thickness R_d should be beneficial.

The same condition in the momentum domain can be expressed as:

$$g(p) = g(p_0)\left.\frac{\mathrm{d}p}{\mathrm{d}R}\right|_{p_0}\frac{\mathrm{d}R}{\mathrm{d}p}, \tag{5}$$

where p_0 is the momentum corresponding to R. Since $g(p_0)\left.\frac{\mathrm{d}p}{\mathrm{d}R}\right|_{p_0}$ is constant, the muon stopping rate remains unchanged whether or not a degrader is used,

$$g(p) \propto \frac{\mathrm{d}R}{\mathrm{d}p} \tag{6}$$

reflects the relationship between the muon's momentum distribution and the rate at which its range changes with momentum.

The red curve drawn in Fig. 8 shows $g(p)$, normalized to $g(p_0)$ at $p_0 = 70$ MeV/c to match the Geant4 calculation. Unless the pion production cross section at 150 MeV/c is 3.38 times higher than that at 70 MeV/c, there are no gains in the muon yield by using a larger radius.

Using the model shown in Eq. (1) and considering the limit of $r_{\mathrm{max}} \to 0$ mm with $f_\pi(r)$ being a delta function, which corresponds to an infinitesimally narrow proton beam, the expected stopped muon yield could be further increased by around 25%. The difference between the ideal value and the updated realistic estimation is only 25%.

7 Conclusion

The COMET experiment aims to search for $\mu^- + N \to e^- + N$ conversion in a nuclear field at J-PARC, utilizing a high-intensity muon beam. In COMET Phase-II, the target sensitivity is estimated to be $\leq 7 \times 10^{-17}$ at 90% C.L. as stated in the CDR [1]. However, recent measurements of the proton-beam emittance in 2018 suggest a significant potential for improvement over the assumptions made in the CDR. The re-optimization of the target size, especially the radius, was performed and resulted in a factor of 1.6 improvement, which seems reasonable.

The analysis of low-energy pion interactions shows that the production of low-energy pions is limited by the compromise between the range–momentum curve of low-energy pions and the initial pion momentum spectrum. Since the pion production at 150 MeV/c is less than 3.38 times that at 70 MeV/c, there is no increase in the muon stopping rate by inserting any materials after pion production.

Considering these findings, further enhancement of the muon stopping yield with a target would not be significant. The optimization strategies presented in this article are quite effective for similar experiments in the high-intensity frontier, offering valuable insights into maximizing lepton production efficiency.

Acknowledgements We wish to acknowledge the support of the COMET group, offering suggestions and encouragement. This work was supported by JSPS KAKENHI Grant Number JP21H04971.

Funding Open Access funding provided by The University of Osaka.

Data Availability Statement All data generated or analyzed during this study are included in this published article.

References

1. Y.G. Cui, et al. The COMET Collaboration. KEK Report 2009-10 (2009)
2. R. Abramishivili, et al. The COMET Collaboration. PTEP 2020, 033C01 (2020)
3. W.H. Bertl et al., Eur. Phys. J. C **47**, 337–346 (2006)
4. B.E. Krikler, *Sensitivity and Background Estimates for Phase-II of the COMET Experiment* (Imperial College, London, 2016)
5. Y. Fukao, et al., in *Proceedings of the 15th Annual Meeting of Particle Accelerator Society of Japan* (2018), pp. 231–234
6. M. Tomizawa, et al., in *Proceedings of the 13th Annual Meeting of Particle Accelerator Society of Japan* (2016), pp. 70–74
7. M.G. Catanesi et al., Eur. Phys. J. C **53**, 177–204 (2008)

8. P. Arve, J. Helgesson. Report Number: Lund-MPh-92/05 (1992)
9. B.W. Allardyce et al., Nucl. Phys. A **209**, 1–51 (1973)
10. T.S.H. Lee, R.P. Redwine, Ann. Rev. Nucl. Part. Sci. **52**, 23–63 (2002)
11. D.E. Groom, N.V. Mokhov, S.I. Striganov, Atom. Data Nucl. Data Tables **78**, 183–256 (2001)
12. D. Ashery, J.P. Schiffer, Annu. Rev. Nucl. Sci. (U. S.) **36**(1), 207–252 (1986)
13. W.R. Leo, *Techniques for Nuclear and Particle Physics Experiments* (Springer, 1994)